Moving Target Simulation of Multi-Band Radar Based on Doppler Frequency Signal Generation Technology

Jiaxing HAO[1], Xuetian WANG[1], Xiaoting SUN[2], Hongmin GAO[1], Le ZOU[1]

[1] Dept. of Integrated Circuits and Electronics, Beijing Inst. of Technology,
Zhongguancun South Street 5, 100081 Beijing, China
[2] Dept. of Mechanical Engineering, Shijiazhuang Vocational College of Technology,
Shibo South Street 1, 050028 Shijiazhuang, China

873328461@qq.com, {1540069244, 1300163339, 2524202998, 1527440170}@qq.com

Abstract. *This paper proposes a corner reflector and Luneburg ball reflector group. The omnidirectional radar cross-sectional (RCS) distribution characteristics of a fighter are simulated using the sharp and smooth RCS distribution features of the corner and the Luneburg ball reflectors, respectively. A new type of Doppler signal generation principle is proposed to design a Doppler frequency simulator to transmit frequency signals by connecting in parallel with the metal layer of the corner reflector and the Luneburg sphere ball, and then transmit through their other end. The existing radar target aircraft cannot simulate the RCS and speed of the targets that are less than 0.005 m² by enhancing the echo intensity of the target location, which makes it impossible for the military to conduct practice drills and evaluate the effectiveness of the air defense systems. The experimental results show that the Doppler frequency simulator successfully simulates the target speed of 0–80 km/h and when the speed is greater than 20 km/h, the error of the simulation frequency is less than 1.5%. The proposed method can provide guidance and a theoretical basis for simulating the speed of various types of aircraft in future work.*

Keywords

Moving target simulation, Doppler frequency, RCS distribution characteristics, corner reflector, Luneburg ball

1. Introduction

A radar target is a target or device with a specifically required RCS distribution or maneuvering characteristics [1]. The RCS distribution characteristics and/or maneuvering characteristics of the simulated target or equipment in the specified space area under the irradiation of the specified frequency radar wave are equivalent to those of the actual target or equipment [2–4]. The traditional radar targets such as a corner reflector and a Luneburg ball reflector cannot be used to simulate complex targets as they can only simulate simple targets and enhance the radar echo intensity [5]. Complex targets can be simulated using Luneburg balls, also known as Luneburg lenses [6]. The outstanding features of a Luneburg ball include a high RCS value and a wide coverage angle of secondary radiation direction. It is mostly used as a stealth material against radars in military fighter jets or military ships. In [7], the University of Electronic Science and Technology of China carried out related optimization research on the layered design of Luneburg balls for Ku, Ka and other frequency bands. Keeping the 1–5 layer dielectric constant unchanged, the winner disc gain was increased by 2 dB and the volume and weight of the Luneburg ball were reduced.

A radar target not only requires simulation of the RCS distribution characteristics of the stationary state of the target, but also needs to consider its speed to simulate. The motion effect is an important issue that needs to be considered in radar systems. In [8], the motion effect was ignored to simplify the algorithm, which caused performance degradation. In [9], a Bayesian method was used to compensate for the motion generated by the object, assuming that its speed was known. Nevertheless, sensor motion processing remains challenging [10]. Especially, when a simulator moves and generates other signals such as interference signals, the relation between the generated Doppler frequency signal and the signal generated by the simulator becomes excessively complicated. In [11], Chen Jingyu et al. designed a computer signal simulation software to simulate a radar-moving target signal and its superposition into the actual radar signal. However, the software was unable to simulate the motion attitude and deal with the background containing white Gaussian noise. In [12], Ding Xiangli et al. designed the microwave circuit of the moving target simulation system using an electrical controller, a splitter, a modulator and other equipment. However, the system was complex and required a connection with the ground computer control system. Hence, the system could not be carried by UAV. In [13], Ma Zhe et al. from the University of Electronic Science and Technology of China, realized the simulation of target speed using FPGA that calculated Doppler frequency according to the

simulated motion speed and the center frequency of the sub-channel, and then used direct digital synthesis (DDS) to generate the corresponding signal and used phase shifter for phase compensation.

Therefore, this paper proposes a new Doppler signal generation method based on the principle of Doppler frequency, which is used to load the corner reflector and Luneburg ball reflector instead of the motion simulator. Subsequently, by designing the angular reflector to simulate the sharp RCS distribution characteristics, and the Luneburg ball reflector to simulate the smooth space RCS distribution characteristics, the simulation of the arbitrary moving target RCS distribution characteristics and speed parameters can be achieved. The proposed method is applied to the actual measurement. It has a low computational complexity, which can simultaneously guarantee performance and reduce cost, and maximize the performance of air defense weapons and combat indicators.

The rest of this paper is organized as follows. Section 2 introduces the generation mechanism of the Doppler shift, the design principle of the oscillating circuit and the principle of the corner reflector and Luneburg ball reflector. Section 3 presents the design scheme and simulation verification of the corner reflector and Luneburg ball. The experiment of Doppler shift corresponding to 0–80 km/h target speed and the experimental verification of a fighter according to the RCS distribution characteristics are presented in Sec. 4. The conclusion and future work are provided in Sec. 5.

2. Dynamic Target Signal Analysis and Simulation Model

2.1 Doppler Signal Generation

When the radar detects a relatively stationary target, the Doppler frequency of the target remains unchanged. However, if the target is moving relative to the radar, there is a frequency difference between the received echo signal and the transmitted signal, which is known as the Doppler frequency shift.

Wen Baojian et al. designed the resonant reflector antenna with characteristics of wide bandwidth, small size and directional radiation [14]. The antenna is suitable for the target simulator with the radial movement of relative detection radar. However, it has the shortcoming of low reflection amplitude.

Liu Yang et al. from Harbin Engineering University designed a corner reflector antenna based on Hilbert classification [15]. The antenna was able to work at the intermediate section of the 8.8 MHz resonance frequency points of the gain of 3.65 dB, its relative bandwidth was higher than 8% and the angle was 180°, with omnidirectional characteristics.

Based on Liu Yang et al. research foundation, the center frequency bandwidth can be adjusted to speed the corresponding Doppler frequency range in order to put the oscillating circuit into the corner reflector. Then the signal source can be assigned to the corner reflector to simulate the speed of the moving target.

Assuming that the target is an ideal target, i.e., the target size is considerably smaller than the radar resolution unit, and the transmitted signal can be expressed as:

$$s(t) = A\cos(\omega_0 t + \phi) \tag{1}$$

where A represents the amplitude of the transmitted signal, ω_0 represents the angular frequency of the transmitted wave signal, and ϕ represents the initial phase. Subsequently, the echo signal received from the moving target can be expressed as:

$$s_r(t) = ks(t - t_r) = kA\cos[\omega_0(t - t_r) + \phi] \tag{2}$$

where k represents the attenuation coefficient and t_r represents the time delay of the radar signal from the transmission to reception.

If the target is stationary, the time delay represented by t_r has a constant value of $2R/c$. If the target moves with a certain speed, the distance R changes with the change of time t, namely:

$$R(t) = R_0 - v_r t. \tag{3}$$

The phase difference can be expressed as:

$$\varphi = -\omega_0 t_r = -\omega_0 \frac{2}{c}(R_0 - v_r t) = -2\pi \frac{2}{\lambda}(R_0 - v_r t). \tag{4}$$

The derivative of the phase difference can be obtained as:

$$f_d = \frac{1}{2\pi}\frac{d\varphi}{dt} = \frac{2}{\lambda}v_r. \tag{5}$$

At this point, the speed of the moving target is:

$$v_r = \frac{f_d \lambda}{2}. \tag{6}$$

Similarly, if the target is stationary, t_r in (2) has a constant value. Consequently, $s_r(t)$ is a fixed value. However, the environment around the target is not static when the target is measured. As an example, if the wind blows the trees, the leaves will produce vibration, or the flowing rivers will produce a large amount of clutter interference, which will affect the Doppler frequency deviation.

When the target is moving, the change of the radial distance between the target and the radar causes the delay τ to change with time, and $\tau(t)$ is used to replace τ. Assume that the radial distance between the target and the radar at the initial time is R_0, the target moves towards the radar with a constant radial velocity v, and the radial distance between the target and the radar is $R(t) = R_0 - vt$. Then the target echo signal at t can be expressed as:

$$S_r(t) = kS_t(t - \tau(t))) =$$
$$K\mu((t - \tau(t))\exp(j2\pi f_0(t - \tau(t))) =$$
$$= \left[\frac{\lambda^2}{(4\pi)^3 R^4 L}\right]^{\frac{1}{2}} G \cdot \gamma \cdot \mu\left(t - \frac{2(R_0 - vt)}{c - v}\right) \cdot \quad (7)$$
$$\exp\left(j2\pi f_0(t - \frac{2(R_0 - vt)}{c - v})\right)$$

where S_t is the transmitted signal, $K = \left[\dfrac{\lambda^2}{(4\pi)^3 R^4 L}\right]^{\frac{1}{2}} G \cdot \gamma$

is the range factor, λ is the signal wavelength, G is the antenna gain, L is the system loss gain, and γ is the complex reflection coefficient.

It can be analyzed from (7) that the target echo signal has an extra target radial velocity v in the frequency domain and a delay v in the time domain compared with the transmitted signal. Therefore, a point target can superimpose a Doppler frequency from the transmitted signal on the frequency, and the amplitude can be reproduced through attenuation factor modulation.

To simulate the Doppler signal, it is necessary to simulate the frequency of the Doppler signal, which is realized by an oscillating circuit in this paper. The oscillating circuit is connected to a corner reflector made of aluminum alloy. For the target aircraft in the simulation exercise, in order to assess whether the air defense forces can accurately detect, we usually plan the trajectory of the simulated target in advance. At this time, we only need to consider the relative flight speed of the target aircraft and adjust it to the corresponding Doppler frequency through the Doppler frequency simulator.

2.2 Oscillation Circuit

Currently, the most widely used sinusoidal oscillators are LC and RC oscillator circuit structures. Figure 1 shows the schematic diagram of an inductive three-point LC oscillation circuit. The oscillation frequency is $f_0 = 1/[2\pi(LC)^{\frac{1}{2}}]$ where $L = L_1 + L_2 + 2M$, and M is the mutual inductance between the inductors L_1 and L_2. Although the circuit structure is tightly coupled, the vibration of the circuit can occur easily and has a high amplitude. A wide range of oscillation frequencies can be obtained by adjusting the capacitance C. However, the oscillation waveform of the circuit is unstable and often contains the influence of high-order harmonics.

Figure 2 shows the schematic diagram of a capacitor-based three-point LC oscillation circuit. The oscillation frequency is $f_0 = 1/[2\pi(LC)^{\frac{1}{2}}]$, where $C = C_1 C_2/(C_1 + C_2)$. Although the oscillating waveform produced by this circuit structure is useful, it is difficult to adjust the frequency of the generated oscillating waveform. Therefore, this circuit is only suitable for a high fixed frequency.

Figure 3 shows the schematic diagram of an RC phase-shifting oscillating circuit. The oscillation frequency
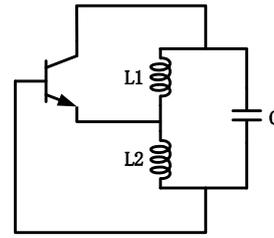

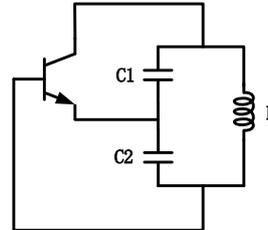**Fig. 1.** AC path diagram of LC inductor three-point oscillator.

Fig. 2. AC path diagram of LC capacitor-based three-point oscillator.
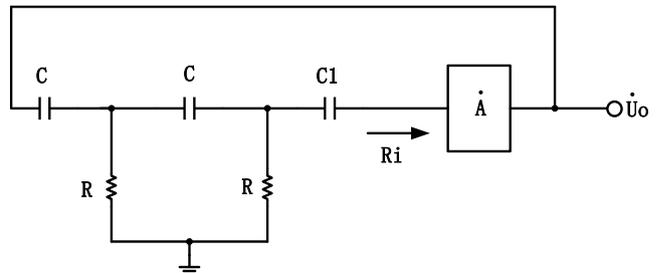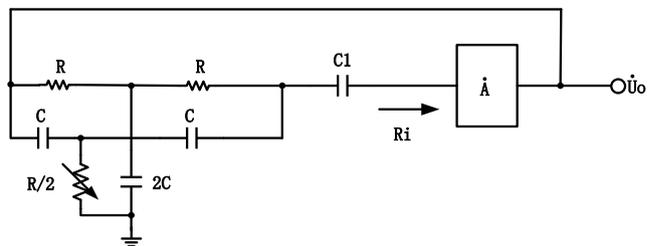

Fig. 3. AC path diagram of RC phase shift oscillator.
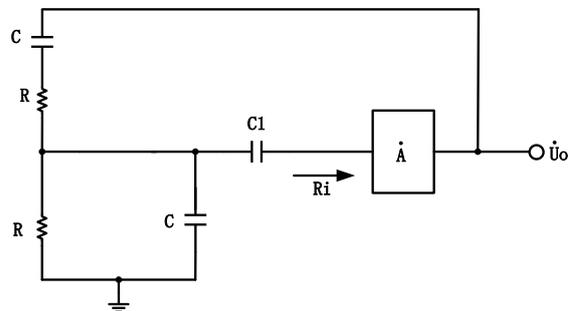

Fig. 4. AC path diagram of RC double T oscillator.

Fig. 5. AC path diagram of RC bridge oscillation circuit.

is $f_0 = 1/[2\pi(6)^{\frac{1}{2}}RC]$. Although this circuit has a simple and economical structure, its frequency selection effect is poor. Its output waveform has an unstable amplitude, large distortion, and inconvenient frequency adjustment, therefore, it is only suitable for use under a fixed frequency.

Figure 4 shows the schematic diagram of an RC double T oscillation circuit, with an oscillation frequency of $f_0 = 1/(5\pi RC)$. This circuit structure has a good frequency and can output a stable sinusoidal waveform. However, the frequency adjustment of the circuit is difficult, so it is not suitable for applications requiring an adjustable frequency.

Figure 5 shows the schematic diagram of an RC bridge oscillation circuit, whose oscillation frequency is $f_0 = 1/(2\pi RC)$. The oscillation waveform output by this circuit structure has a stable frequency and no distortions. The amplitude of the output waveform can be stabilized by adding negative feedback. Furthermore, it is relatively simple to change the oscillation frequency, which makes it suitable for applications requiring an adjustable frequency.

To sum up, it is difficult to use the LC oscillation circuit to generate stable sinusoidal waves with an adjustable frequency. It is more suitable for generating high-frequency oscillation signals above 1 MHz. On the other hand, the RC oscillation circuit is more suitable for generating oscillation signals with a frequency below 1 MHz. According to the calculations, the corresponding Doppler frequency of the fighter is 45 kHz, when the radar is scanning at 24 GHz CW dot frequency, which is less than 1 MHz. Therefore, the RC oscillation circuit is adopted in this paper, and the corresponding circuit schematic diagram is shown in Fig. 6.

In the sinusoidal oscillation circuit shown in Fig. 6, whose oscillation frequency is $f_0 = 1/(2\pi RC)$, R_1, C_1, R_2 and C_2 constitute a serial-parallel frequency selection network as the positive feedback network of the circuit. Furthermore, R_3, R_4 and R_5 constitute the negative feedback amplification network of the circuit. The two diodes constitute a nonlinear network, which can render the amplifier of the circuit stable over 3 times. This prevents the distortion of the output waveform and ensures its stability. The opamp uses LF356n. Since it is a single-stage common emitter amplifier circuit, the output voltages of the transistor VT U_0 and U_i are 180° in phase. When the output voltage passes through the RC network, it becomes the feedback voltage and then sends it to the input end.
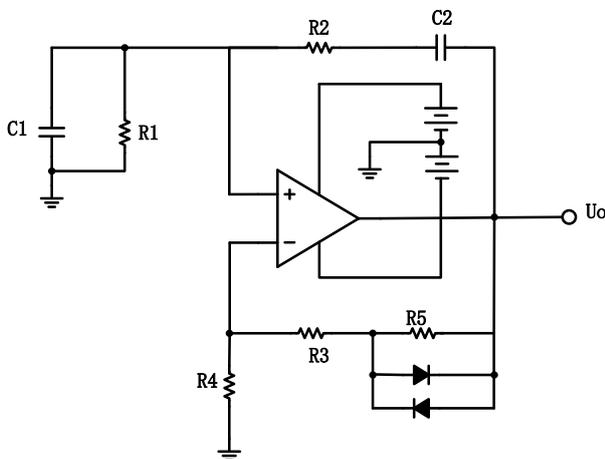

Fig. 6. Design of Doppler frequency simulator.

When the output voltage signal of oscillation is zero, the voltage on the diode is very small and the resistance is very large, which makes the negative feedback the weakest. Therefore, the positive feedback is the strongest on the whole, and the voltage of the output signal increases rapidly. When the output voltage reaches above 0.5 V, the diode is gradually switched on, and the negative feedback effect is gradually reflected and strengthened. Hence, the increase in the voltage of the output signal is reduced, and the amplitude is controlled with the potentiometer.

2.3 Corner Reflector and Luneburg Ball Reflector

An angular reflector is usually composed of two or three mutually orthogonal metal plates. There are three planes at the opposite angles of the three sides, which form a strong triple internal reflection. Consequently, a very wide scattering pattern is formed in the solid space. The inverse RCS values of the three sides of an isosceles right triangle can be calculated as:

$$\sigma = 10\lg\frac{4\pi a^4}{3\lambda^2} \qquad (8)$$

where a is the right-angle side length, and σ is the RCS area with units of dBsm. Under far-field and high-frequency conditions, the general calculation formula of the scattering field in the far-field region of the surface of an object is as follows according to the Stratton-Chu integral equation:

$$E^s(r) = \frac{jk}{4\pi}\frac{e^{-jkr}}{r}\int_\Omega i(\mathbf{M}_s(r') + Z_0\mathbf{s}\mathbf{J}_s(r')\exp(jkr'(\mathbf{s}-\mathbf{i}))\,d\omega \qquad (9)$$

In (9), $\mathbf{i}$ and $\mathbf{s}$ are unit vectors of the incident and receiving directions, respectively, Z_0 is the wave impedance in free space, Ω is the cross-sectional area of the incident wave illuminated on the object surface, and $\mathbf{J}_s(r')$ and $\mathbf{M}_s(r')$ are current and magnetic flow vectors, respectively.

According to (9), if the included angle of the two metal plates of the angle reflector is reduced, the vector difference between $\mathbf{i}$ and $\mathbf{s}$ will be reduced accordingly. Corresponding to $\mathbf{s} - \mathbf{i}$, the range of stationary space angle corresponding to the angle reflector will be reduced. Subsequently, the RCS value will be reduced accordingly, which can better conform to the RCS distribution characteristics of the sharp angle of the target such as the fifth generation to be simulated. For example, the nose and tail of fighter F16 are designed to be sharper to reduce wind resistance. At the same time, the absorbing material is coated to reduce the RCS. The RCS of the nose is only 7 dBsm, and the angle range of 3 dB drop is only ±7°, a total of 14°. However, the 3dB fluctuation range of the ordinary straight angle reflector is −25° to 25°, which cannot meet the simulation demand. According to (9), the 3dB fluctuation range angle of the angle reflector can be reduced accordingly until ±7°.

The outer reflection of the Luneburg ball reflector is consistent with that of the sphere. However, the radar reflection intensity is weaker than that of the right-angle trihedral reflector. The Luneburg ball reflector causes a specular reflection on the side of the coming wave and the inner layer of the Luneburg ball is filled with material of different dielectric constants. Therefore, an incoming wave reaches its metal reflection surface through constant refraction and is then reflected to the radar system, in a direction that is opposite to the direction of the coming wave.

The Luneburg ball refractive index n is a function of distance r from the center of the sphere to a point on the surface of the sphere. It can be written as:

$$n(r) = \sqrt{2 - \left(\frac{r}{R}\right)^2} \qquad (10)$$

where r represents the distance from the center of the sphere to a point on the outer surface of the dielectric sphere and R represents the radius of the Luneburg ball. The dielectric constant of each dielectric sphere layer is:

$$\varepsilon(r) = n(r)^2 = 2 - \left(\frac{r}{R}\right)^2. \qquad (11)$$

In the actual manufacturing of the Luneburg ball, it is not possible to achieve a gradual change of dielectric constant from the outermost layer to the inner layer. Therefore, using several layers of materials with decreasing dielectric constants can meet the basic requirements.

The Luneburg ball used in this paper is made of nylon material for 3D printing processing. Nylon has high rigidity and flexibility. When the printed item is thin, nylon shows good flexibility. When the item is thick, nylon shows good rigidity and has good corrosion resistance. The density of nylon is modified according to the relative dielectric constant of each layer, and the outermost layer is made of fiberglass steel.

3. Simulation Design

The FEKO simulation software is used to design diagonal and Luneburg ball reflectors and gets their distribution characteristics. Considering that the corner reflector should be connected to the oscillating circuit in parallel as an antenna, a diagonal reflector is required for the slit design. In this design, the triangle side length, gap width and pitch angle are set to be 150 mm, 2.25 mm and 55°, respectively, which are shown in Fig. 7. Figure 8 shows the effect of different gap widths on the performance of diagonal reflectors.

A bracket is added between every two plates of the corner reflector, which is made of PVC wave-passing material to reduce the interference of the diagonal reflector, as shown in Fig. 7(b). The thickness and the length of the triangle plate are 3.6 mm and 150 mm, respectively, and the
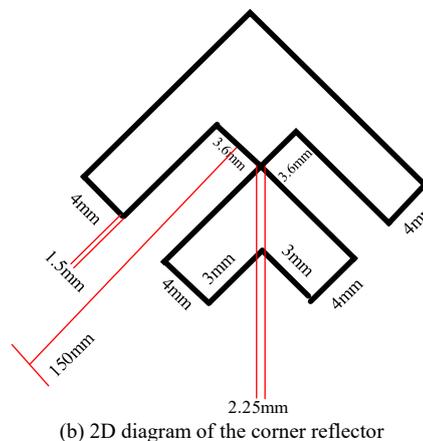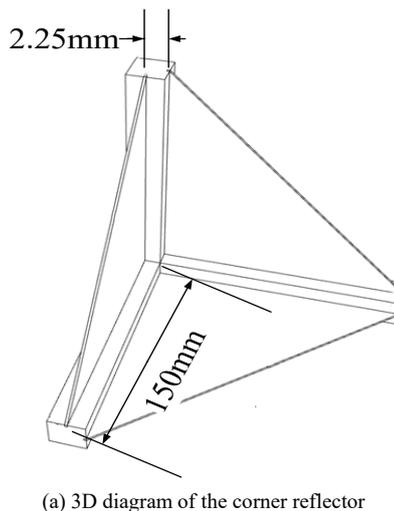

(a) 3D diagram of the corner reflector

(b) 2D diagram of the corner reflector

Fig. 7. Triangular trihedral corner reflector.

material is an aluminum-plastic plate. The thickness of the medium of the 3D printing material is 1.5 mm. Thus, the spacing between the two gaps can be obtained as $1.5(2)^{1/2} = 2.25$ mm. According to (8), the theoretical RCS value $\sigma_{\max} = 10 \lg(4\pi a^4/(3\lambda^2)) = 10 \lg(4\pi \times 0.15^4/(3 \times 0.0125^2)) = 10.9$ dBsm of an angular reflector with a side length of 150 mm can be calculated.
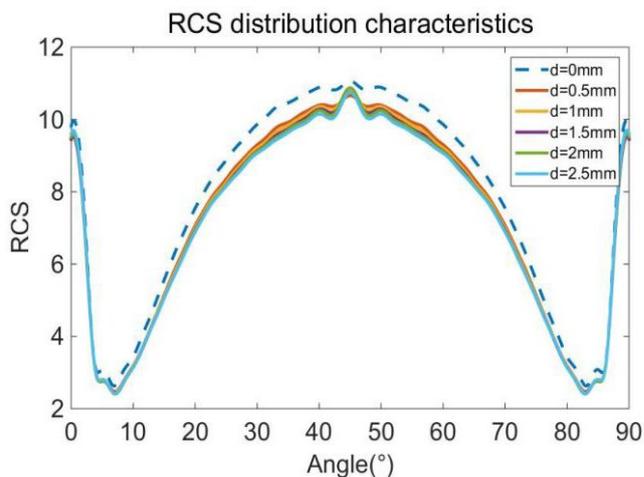

Fig. 8. Radar cross-section distribution characteristics of the corner reflector when the pitch angle is equal to 55°.

Figure 8 shows that the maximum value of RCS of the corner reflector is 11 dBsm, which is consistent with the theoretical calculation of (8). When the gap width is less than 2.5 mm, the RCS value decreases slightly. However, the distribution characteristics of RCS remain consistent. The included angle between the two sides is changed to 45°, and the size is changed to 200 mm, as shown in Fig. 9.

As Figure 10 shows, the fluctuation range of 1dB RCS value in the horizontal azimuth plane is about 13° between 16° and 29°, and that in the pitching plane is about 25° between 46° and 71°. The fluctuation range of the RCS value in the horizontal azimuth plane is about 20° between 13° and 33°, and that in the pitching plane is about 30° between 45° and 75°. This kind of angle inversion can simulate the RCS distribution characteristics within the sharp angle range. Thus, the angle range of ±10° is selected as the simulated target, and the other parts are endowed with absorbing materials. The Luneburg ball is irradiated by a far-field plane wave with a frequency of 24 GHz. The scanning angle ranges are 0° and between –90° and 90°in the azimuth and elevation dimensions, respectively, and the angular scanning interval is 0.1°, as shown in Fig. 11.

The Luneburg ball simulation structure consists of three dielectric layers and an outermost air layer. The relative permittivity of the dielectric layer can be calculated using (11). Table 1 shows the specific design parameters.
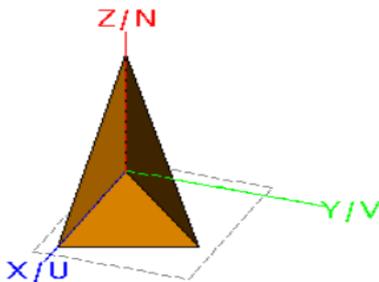

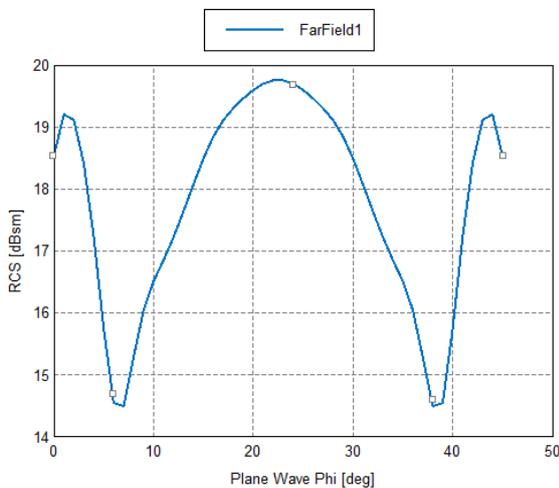**Fig. 9.** Corner reflector with a side angle of 45°.

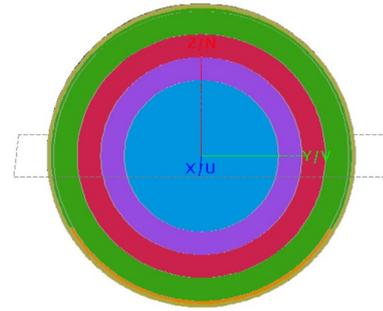**Fig. 10.** Radar cross-section distribution characteristics with a pitch angle of 55°.

Fig. 11. Simulation structure of the Luneburg ball reflector.

Layer	Medium reflectance	Relative permittivity	Medium layer thickness [mm]
1	1.4	1.96	22
2	1.34	1.7956	6
3	1.22	1.4884	6
4	1	1.153	6

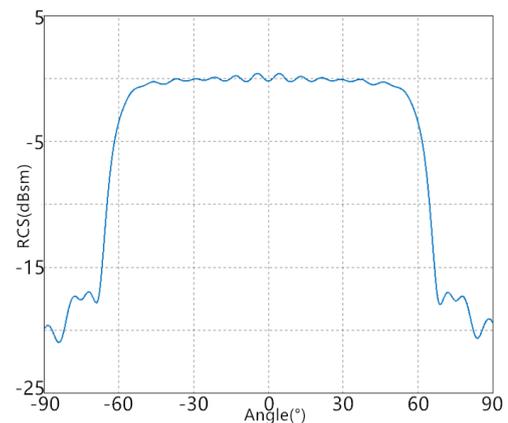**Tab. 1.** Design of the dielectric constant of each layer of the Luneburg ball.

Fig. 12. Radar cross-section distribution characteristics of the Luneburg ball.

Figure 12 shows the simulation results obtained after using the relevant parameters of the Luneburg ball provided in Tab. 1. It can be seen from Fig. 12 that the maximum value of the RCS of the Luneburg ball is about 0 dBsm. The RCS value of the Luneburg ball reflector is relatively stable within the range of 112° between –56° and 56° in the pitching azimuth plane, and the fluctuation of this range is less than 3 dBsm. Nevertheless, the RCS value is still stable at around 0 dBsm. The width of the coverage angle in the secondary scattering direction can be changed by changing the size and position of the metal reflecting plate. Therefore, the size of the Luneburg ball and the design of the metal reflecting plate can be changed to satisfy the required RCS distribution characteristics of the angle range of the stationary space of the target. The other angles that do not need to reflect echo are filled with absorbing materials. In this way, a finite number of corner reflectors and Luneburg balls can be selected to form an array to

simulate the corresponding target based on the RCS distribution characteristics of the target to be simulated.

4. Experimental Verification

4.1 Doppler Frequency Measurement Test

To evaluate the performance of the Doppler frequency simulator, a 24 GHz frequency test system is designed for experimental verification, as shown in Fig. 13. A speed of 0–80 km/h is simulated, divided into six levels: 0 km/h, 5 km/h, 10 km/h, 20 km/h, 40 km/h and 80 km/h. According to (6), the corresponding analog frequencies can be calculated at 0, 220 Hz, 440 Hz, 880 Hz, 1.7 kHz, and 3.6 kHz. The voltage of the 3.6 kHz oscillation circuit is ±9 V, R_1 and R_2 are equal to 72 kΩ, C_1 and C_2 are equal to 0.01 μF, R_3 is 18 kΩ, R_4 is 10 kΩ and R_5 is equal to 3 kΩ.

The computer sends the corresponding instruction statements through a serial debugging assistant software to control the start of RF transceiver components and the setting of parameters. The waveguide horn antenna has the advantages of a wide working band, good directivity, large power capacity, good radiation characteristics and high gain. Therefore, the horn antenna is used as the transceiver antenna of the test system. The vector network analyzer sets the transmitting continuous wave point frequency. According to the Nyquist sampling theorem $f_s > 2f_N$. The specific parameters are shown in Tab. 2. The Doppler frequency test results are shown in Fig. 14.
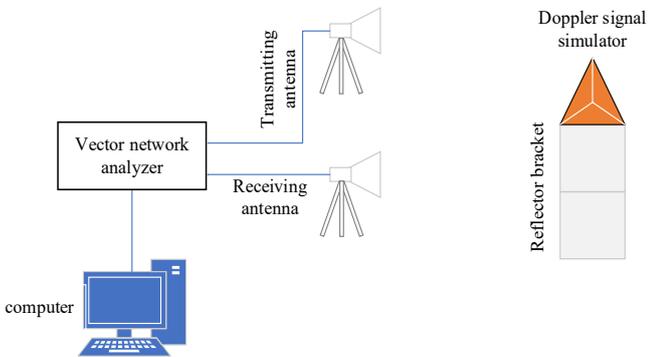

Fig. 13. Doppler frequency test system.

| Parameter name	Parameter value
The highest frequency in the signal (f_N)	3.6 kHz
Sampling frequency(f_s)	10 MHz
Amplification power	20 dB
Collection points	361
IF bandwidth	50 kHz

Tab. 2. Parameter settings.

Figure 14 shows that the simulated Doppler frequency components appear on the processed spectrum, which verifies the effectiveness and accuracy of the Doppler frequency simulator proposed in this paper. Table 3 shows the errors of the proposed Doppler frequency simulator. It can be seen from the table that the test errors at 5 km/h and 10 km/h are relatively high. This is because the vector network analyzer collects the data at a frequency of about 700 Hz. The level position above 20 km/h has a minor influence and the error is less than 2%, which meets the test accuracy requirements.
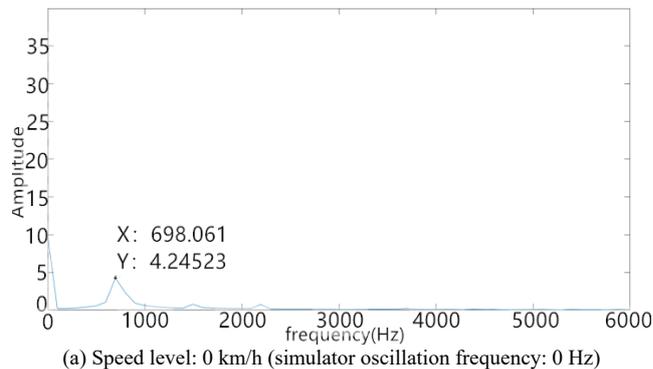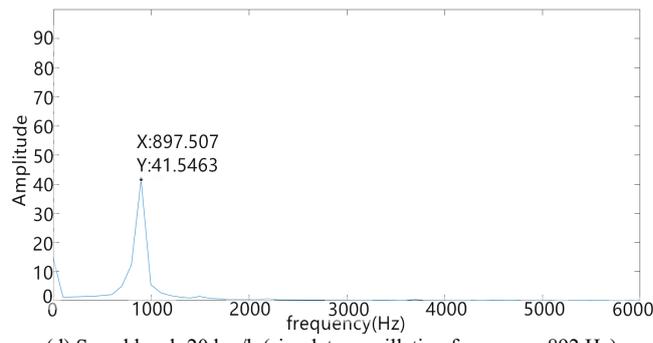

(a) Speed level: 0 km/h (simulator oscillation frequency: 0 Hz)
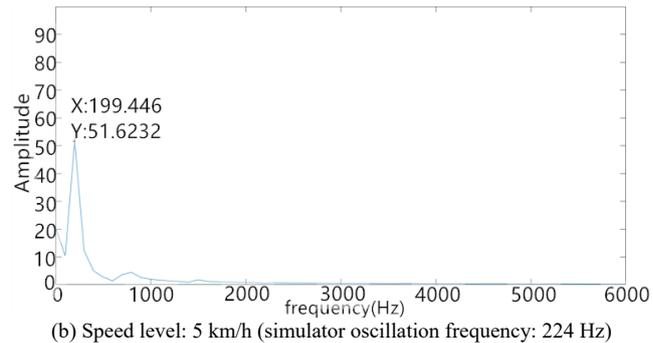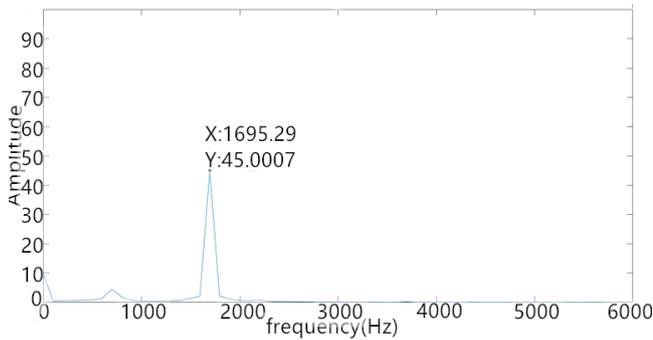

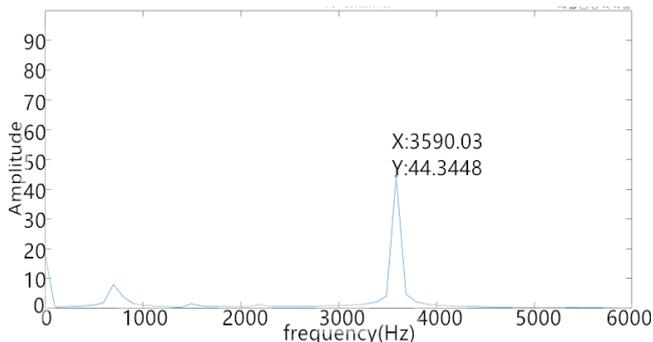(b) Speed level: 5 km/h (simulator oscillation frequency: 224 Hz)
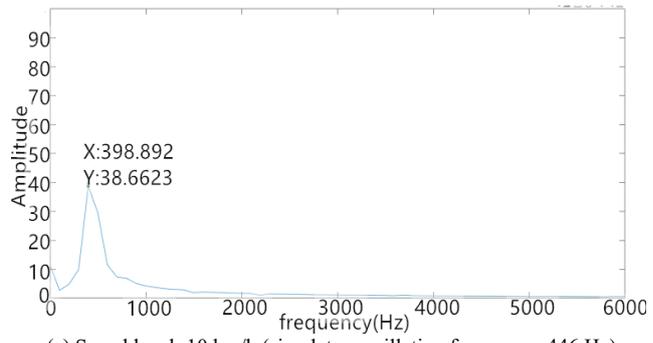
(c) Speed level: 10 km/h (simulator oscillation frequency: 446 Hz)

(d) Speed level: 20 km/h (simulator oscillation frequency: 892 Hz)

(e) Speed level: 40 km/h (simulator oscillation frequency: 1.70 kHz)

(f) Speed level: 80 km/h (simulator oscillation frequency: 3.60 kHz)

Fig. 14. Test results of Doppler frequency simulator.

Speed level [km/h]	0	5	10	20	40	80
Simulator frequency deviation	0%	10.96%	10.76%	0.62%	0.29%	0.27%

Tab. 3. Error analysis of Doppler frequency shift simulator.

4.2 Simulation and Test Results of Corner Reflector and Luneburg Ball Reflector

A certain type of fighter aircraft is modelled using the FEKO, as shown in Fig. 15. The incident wave frequency is set to 24 GHz for an ideal plane wave and the far-field beam irradiation range is: azimuth dimension of 0°−360°, 90° pitch dimension, and angle scan interval of 1°.

Figure 16 shows the simulation results at 24 GHz frequency. The maximum RCS of this fighter is about 3 dBsm, and there are two strong scattering centers at 0° and 180° azimuth angles of the horizontal azimuth plane, both of which are about 2 dBsm. The angle range of the RCS that drops 10 dBsm is about 10°. There are two secondary strong scattering centers at 90° and 270°, with RCS values of about –16 dBsm, and the angle range of RCS that drops 10 dBsm is about 20°. The RCS values in other azimuth ranges are generally low, mostly below –35 dBsm.

The simulation results show that the simulated regions are mainly divided into two categories: 1) very large RCS values in narrow regions and, 2) very small RCS values and large fluctuations in wide regions. The corner reflector has a very large RCS value. However, the coverage
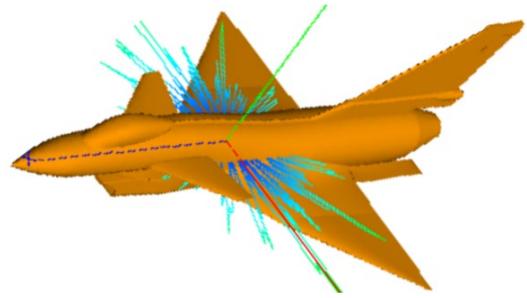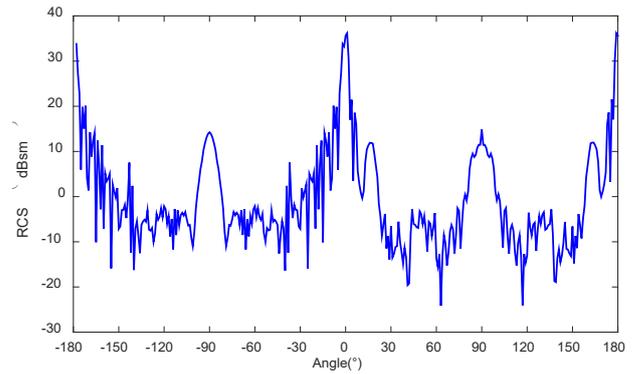

Fig. 15. Structure of a fighter model.

Fig. 16. Radar cross-section distribution characteristics of a fighter aircraft.
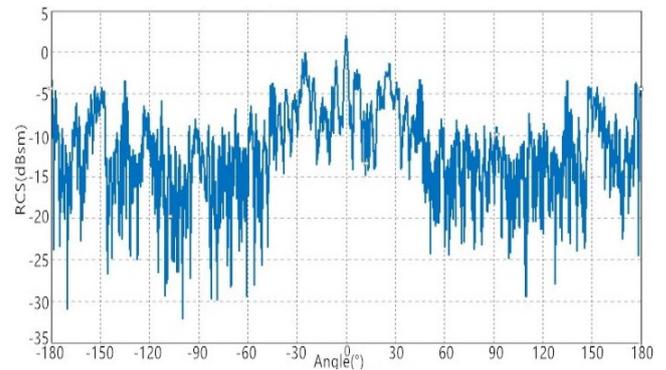

Fig. 17. Radar cross-section distribution characteristics of the array of corner reflectors and Luneburg balls.

angle range of the quadratic directional scattering is extremely wide. Therefore, the structural variation of the corner reflector is considered to meet the requirements of a large RCS value and a narrow coverage angle range of the quadratic directional scattering. The Luneburg ball reflector has a wide coverage angle in the secondary scattering direction, which can be used to simulate the smooth RCS distribution characteristics of area 2 in Fig. 16. The combination is composed of four corner reflectors and four Luneburg ball reflectors. The included angle of the corner reflector near 0° is controlled at about 20–30°, and the test results are shown in Fig. 17.

Figure 17 shows that a peak appears near 0°, and its RCS value is roughly the same as that of Fig. 16. The spikes corresponding to –90° and 90° are also simulated accordingly, which completes the simulation of RCS distribution characteristics proposed in this paper.

5.   Conclusion and Future Work

In this paper, a moving target simulation of multi-band radar based on Doppler frequency signal generation technology is proposed to simulate the target velocity. The feasibility of the proposed method is verified by testing the oscillation circuit simulating the target speed of 0–80 km/h. Based on the simulation of the Doppler frequency signal and the simulation of the RCS distribution characteristics of a fighter jet, the following conclusions can be drawn:

- A Doppler simulator designed by the RCS bridge oscillation circuit was used to simulate the Doppler frequency. When the simulation speed exceeded 20 km/h, the error of the simulation frequency was less than 1%. Thus, the oscillation circuit proposed in this paper can simulate the moving target of 0–80 km/h.

- By changing the size of the corner reflector and the included angle of two metal plates on both sides, the RCS distribution characteristics of the sharp angle of the target were simulated.

- By changing the size and position of the Luneburg ball reflector, the RCS distribution characteristics of the stationary spatial angle of the target were simulated.

- However, the normal speed of most aircrafts is far more than 80 km/h. Therefore, future work will include changing the amplifier parameters, capacitance and resistance in the oscillation circuit to conform to the frequency corresponding to the aircraft speed and analyzing the possible error caused by the frequency.

References

[1] ZHANG, Y., HO, K. C. Multistatic localization in the absence of transmitter position. *IEEE Transactions on Signal Processing*, 2019, vol. 67, no. 18, p. 4745–4760. DOI: 10.1109/TSP.2019.2929960

[2] ZHAO, L., YANG, Y., XIA, Y., et al. Active disturbance rejection position control for a magnetic rodless pneumatic cylinder. *IEEE Transactions on Industrial Electronics*, 2015, vol. 62, no. 9, p. 5838–5846. DOI: 10.1109/TIE.2015.2418319

[3] BUCHANAN, N. B., FUSCO, V. F. A simple measurement technique for accurate bistatic retrodirective radiation pattern calculation based on the active element pattern method. *IEEE Transactions on Antennas and Propagation*, 2018, vol. 66, no. 1, p. 472–475. DOI: 10.1109/TAP.2017.2776611

[4] LOPEZ-PASTOR, J. A., ARQUES-LARA, P., FRANCO-PENARANDA, J. J., et al. Wi-Fi RTT-based active monopulse RADAR for single access point localization. *IEEE Access*, 2021, vol. 9, p. 34755–34766. DOI: 10.1109/ACCESS.2021.3062085

[5] IBERLE, J., RIPPL, P., WALTER, T. A near-range radar target simulator for automotive radar generating targets of vulnerable road users. *IEEE Microwave and Wireless Components Letters*, 2020, vol. 30, no. 12, p. 1213–1216. DOI: 10.1109/LMWC.2020.3030231

[6] BOSILJEVAC, M., CASALETTI, M., CAMINITA, F., et al. Non-uniform metasurface Luneburg lens antenna design. *IEEE Transactions on Antennas and Propagation*, 2012, vol. 60, no. 9, p. 4065–4073. DOI: 10.1109/TAP.2012.2207047

[7] PFEIFFER, C., GRBIC, A. A printed, broadband Luneburg lens antenna. *IEEE Transactions on Antennas and Propagation*, 2010, vol. 58, no. 9, p. 3055–3059. DOI: 10.1109/TAP.2010.2052582

[8] LIU, P., ZHU, X. W., ZHANG, Y., et al. 3D-printed cylindrical Luneburg lens antenna for millimeter wave applications. *International Journal of RF and Microwave Computer-Aided Engineering*, 2020, vol. 30, no. 1, p. e21994.1–e21994.8. DOI: 10.1002/mmce.21994

[9] LI, Z. S., DOSSO, E., SUN, D. Motion-compensated acoustic localization for underwater vehicles. *IEEE Journal of Oceanic Engineering*, 2016, vol. 41, no. 4, p. 840–851. DOI: 10.1109/JOE.2015.2503518

[10] WEBSTER, S. E., EUSTICE, R. M., SINGH, H., et al. Advances in single-beacon one-way-travel-time acoustic navigation for underwater vehicles. *International Journal of Robotics Research*, 2012, vol. 31, no. 8, p. 935–950. DOI: 10.1177/0278364912446166

[11] CHEN, J. Y., LIU, Y. P. Doppler radar moving target signal simulation software design. *Journal of Electronic Countermeasures*, 2006, vol. 2, no. 3, p. 34–36. (In Chinese)

[12] DING, X. L. Design and implementation of target dynamic simulator. *North China University of Technology*. Beijing (China), 2010. (In Chinese)

[13] MA, Z. *Broadband High-Speed Target Echo Simulation System Design and Implementation. Master's Theses*. University of Electronic Science and Technology, Chengdu (China), 2021. (In Chinese)

[14] BIE, S., PU, S. Array design of 300 GHz dual-band microstrip antenna based on dual-surfaced multiple split-ring resonators. *Sensors*, 2021, vol. 21, p. 1–13. DOI: 10.3390/s21144912

[15] LIU, Y. Research on small marine antenna in medium and short wave segment. *Harbin Engineering University*, Harbin (China), 2011. (In Chinese)